Journal of Power Sources 195 (2010) 6323–6328

Contents lists available at ScienceDirect

Journal of Power Sources

journal homepage: www.elsevier.com/locate/jpowsour

Stable support based on highly graphitic carbon xerogel for proton exchange membrane fuel cells

Hong Jin[a,b], Huamin Zhang[a,*], Yuanwei Ma[a,b], Ting Xu[a,b], Hexiang Zhong[a], Meiri Wang[a]

[a] PEMFC Key Materials and Technology Laboratory, Dalian Institute of Chemical Physics, Chinese Academy of Sciences, Dalian 116023, China
[b] Graduate School of the Chinese Academy of Sciences, Beijing 100039, China

ARTICLE INFO

Article history:
Received 18 March 2010
Received in revised form 16 April 2010
Accepted 16 April 2010
Available online 22 April 2010

Keywords:
Proton exchange membrane fuel cells
Carbon xerogel
Carbon support
Durability
Accelerated aging test

ABSTRACT

Highly graphitic carbon xerogel (GCX) is prepared by the modified sol–gel polymerization process using cobalt nitrate as the catalyst, followed by high temperature treatment at 1800 °C. The as-prepared GCX is explored as a stable support for Pt in proton exchange membrane fuel cells. The results of N_2 sorption measurement and X-ray diffraction analysis (XRD) reveal that GCX has a better mesoporous structure and a preferably higher degree of graphitization, compared with the commercial XC-72 carbon black. The transmission electron microscopy (TEM) image indicates that Pt nanoparticles are well dispersed on GCX and exhibit relatively narrow size distribution. Accelerated aging test (AAT) based on potential cycling is used to investigate the durability of the as-prepared Pt/GCX in comparison with the commercial Pt/C. Electrochemical analysis demonstrates that the catalyst with GCX as a support exhibits an alleviated degradation rate of electrochemical active surface area (39% for Pt/GCX and 53% for Pt/C). The results of single cell durability tests indicate that the voltage loss of Pt/GCX at 100 mA cm^{-2} is about 50% lower than that of Pt/C. GCX is expected to be a corrosion resistant electrocatalyst support.

1. Introduction

Proton exchange membrane fuel cells (PEMFCs), as the ideal power source conversion plants for stationary and transportation applications, have been investigated quite intensively over the past decades. Electrocatalyst support, which is used to decrease the usage of platinum and increase the utilization of electrocatalyst, is becoming one of the key materials in PEMFCs. At the same time, its properties directly affect the performance and the durability of fuel cells [1–5]. In the adverse operating conditions of PEMFCs, such as the acidic environment, the high potential condition and the presence of Pt [6], Vulcan XC-72 carbon black (Cabot Corp., denoted as XC-72) widely used as electrocatalyst support can be easily oxidized and degraded [7]. Therefore, the supported nanoparticles usually agglomerate and detach from the corroded sites resulting in the decrease of the electrochemical active surface area (EASA) [1,3–5]. Generally, there are two approaches to tackle the support corrosion: one is introducing non-carbon supports [8–10] and the other is developing novel carbon materials [11–18]. Although Pt supported on non-carbon catalysts show a better stability than conventional Pt/C catalyst [8–10], the corresponding catalytic activities are much lower due to the low conductivity of the non-carbon supports. Up to now, carbon material is still believed to be the best choice for PEMFCs support because of its superior properties including high electronic conductivity, proper surface property, low cost and abundant anchor sites for catalyst particles [1].

Recently, a number of novel carbon materials have been investigated as supports in PEMFCs, such as ordered mesoporous carbon [11], carbon nanotubes [12,13], carbon nanohorns [14,15], carbon nanocoils [16–18], graphitic carbon [19] and carbon aerogels [20,21]. Carbon aerogels have received considerable attention due to their particularly controllable pore structures including high porosities, surface areas and appropriate pore volumes [20,21]. However, because of the high cost of supercritical drying method, their practical application in PEMFCs has been greatly restricted. Carbon xerogel [22], obtained by vacuum drying instead of complicated supercritical drying, is one of the promising novel carbon supports for fuel cell catalyst due to its appropriate porous structure similar to carbon aerogel [20,21] and simple drying method for industrial and domestic application. As a kind of carbon materials, carbon xerogels suffer the same corrosion problems as XC-72 because of their low degree of graphitization. Generally, the degree of graphitization is mainly determined by the temperature of heat-treatment. At the same time, the high temperature calcination also leads to the decrease of the specific surface area and the collapse of the mesostructure. Therefore, it is expected to be a serious barrier to obtain a highly stable carbon xerogel with porous properties and relatively high specific surface areas.

Carbon aerogels with relatively high specific surface areas can be obtained when transition metal salts are used as catalyst in the

* Corresponding author. Tel.: +86 411 84379669; fax: +86 411 84665057.
E-mail address: zhanghm@dicp.ac.cn (H. Zhang).

0378-7753/$ – see front matter © 2010 Elsevier B.V. All rights reserved.
doi:10.1016/j.jpowsour.2010.04.050

process of porous structure formation and graphitization [23–25]. In this work, the graphitization process carried out with aid of catalysts was introduced into carbon xerogels preparation. A kind of highly graphitic carbon xerogels was prepared by pyrolyzing the cobalt nitrate doped polymeric precursor at high temperature and applied as a stable catalyst support in PEMFCs. Cobalt species deposited on the pyrolized sample were removed by 0.5 M H_2SO_4. Pt supported on the as-prepared graphitic carbon xerogel (Pt/GCX) was prepared by the ethylene glycol (EG) reduction method in comparison with a conventional Pt/C catalyst (Johnson Matthey Corp., 20 wt.%). In electrochemical measurements and single cell tests, accelerated aging tests (AATs) were used to evaluate the stability of catalysts.

2. Experimental

2.1. Synthesis of GCX support

The RF-Co xerogel was synthesized by the sol–gel polymerization of resorcinol (R) and formaldehyde (F) in water with an appropriate amount of cobalt nitrate as catalyst. In brief, the stoichiometric R/F molar ratio was 1:2. At first, cobalt nitrate was added into the solution and the molar ratio of resorcinol (R) to catalyst (C) was 32:1. The solution was kept stirring until it turned to RF aquagel. The RF aquagel was dried and cured in vacuum oven at 85 °C for 7 days. Then, the as-prepared xerogel was carbonized at 1000 °C for 3 h and then at 1800 °C for 2 h in nitrogen flow. After that, the product was mulled and then stirred in 0.5 M H_2SO_4 solution to remove the soluble Co species. At last, after being washed to neutral with deionized water and dried in vacuum oven at 60 °C, the resulting carbon xerogel was obtained and identified as GCX.

2.2. Preparation of Pt/GCX catalyst

The Pt/GCX catalyst was synthesized by reducing H_2PtCl_6 in a mixture of ethylene glycol (EG) using the as-prepared GCX powder as support. The synthesis procedure for the 20 wt.% Pt/GCX catalyst was as follows: 133.3 mg GCX was added into 50 mL EG and the mixture was homogenized for 20 min in an ultrasonic bath, followed by the addition of 2.26 mL H_2PtCl_6/EG solution (0.075 M). Then, a certain amount of NaOH/EG solution was dripped into the mixture to adjust the pH to greater than 10. The reduction procedure was conducted at 130 °C with reflux for 2.5 h. After being washed with deionized water and dried in vacuum oven at 60 °C, the Pt/GCX catalyst was finally obtained.

2.3. Physical characterization of supports and catalysts

X-ray diffraction (XRD) analysis were performed on Rigaku Rotalflex (RU-200B) using Cu-Kα radiation (λ = 1.54056 Å) with a Ni-filter to characterize the crystalline structures of samples. The 2θ angular region was extended from 20° to 90°, and the scan rate was 5° min^{-1} with a step size of 0.02°. In the X-ray diffraction data, the average particle size of the Pt particles could be estimated from Pt (2 2 0) diffraction peak [26].

BET analysis were carried out by physical adsorption of N_2 at 77 K using a Micromeritics Accelerated Surface Area and Porosimetry System (ASAP2010). The Brunauer–Emmett–Teller (BET) equation was applied to obtain the specific surface area. And the Barrett–Joiner–Halenda (BJH) method provided the pore size distribution (PSD).

Inductively coupled plasma-atomic emission spectroscopy (ICP-AES) analysis of the dissolved GCX sample was conducted to determine bulk Co content.

Transmission electron microscopy (TEM) measurements were conducted on a JEOL JEM-2011 electron microscope operated at 100 kV. The catalyst was placed in a vial containing ethanol and then ultrasonically agitated to form homogeneous suspension. A drop of the suspension was dispersed on a copper grid for analysis. Two hundreds of metal particles were sampled to obtain the particle distribution diagram of the catalyst.

2.4. Electrochemical measurements of catalysts

2.4.1. Cyclic voltammetry (CV) measurements

Electrochemical characterization was performed on CHI 600 electrochemical station (CH Instrument, USA) with an RDE system (EG&G model 636, USA). The commercial Pt/C catalyst (JM Corp., 20 wt.%) was used as the comparison. The Pt/GCX and Pt/C (20 wt.%) electrocatalysts were tested in 0.5 M H_2SO_4 electrolyte with a standard three-electrode electrochemical cell in which a Pt foil (3 cm^2) and a saturated calomel electrode (SCE) served as the counter electrode and the reference electrode, respectively. The thin film catalyst layer on the glassy carbon electrode (GCE, area: 0.1256 cm^2) which was used as working electrode was prepared as follows. A mixture containing 5 mg Pt/GCX or commercial Pt/C (20 wt.%) catalyst, 1 mL ethanol and 50 μL Nafion (Du Pont Corp., 5 wt.%) was ultrasonically blended for 20 min to obtain a homogeneous ink. 10 μL of the mixture was cast on the clean GCE surface and dried in air. Durability tests of catalyst were performed by a potential cycling accelerated aging test. The 1000 cycles CV data were recorded in 0.5 M H_2SO_4 electrolyte purged with N_2 at room temperature. The potential range was from 0 to 1.2 V and the scan rate was 50 mV s^{-1}. All electrode potentials in this paper were quoted to reversible hydrogen electrode (RHE).

2.4.2. Rotating disk electrode (RDE) tests

A rotating disk electrode (RDE) system (EG&G model 636) coupled with CHI 600 electrochemical station (CH Instrument, USA) was used to test the activities of the catalysts. The RDE tests were carried out in O_2 saturated 0.5 M H_2SO_4 solution with the rotating speed of 1600 rpm, the potential range from 1.15 to 0.05 V, and the scan rate of 5.0 mV s^{-1}.

2.5. Cell tests of Pt/GCX and Pt/C catalysts

2.5.1. Preparation of membrane electrode assembly (MEA)

The as-prepared Pt/GCX and Pt/C (20 wt.%) were tested as PEMFCs cathode catalyst with Pt loading of 0.3 mg cm^{-2}. In all cases, the commercial Pt/C catalyst (TKK Corp., 47.6 wt.%) with Pt loading of 0.3 mg cm^{-2} was used as the anode catalyst and Nafion 212 (Du Pont Corp.) was used as the proton exchange membrane. Taking the Pt/GCX as an example, the electrode was prepared as follows: the as-prepared Pt/GCX catalyst was mixed with appropriate amount of isopropyl alcohol and 10 wt.% PTFE emulsion (the weight ratio of Pt/GCX to PTFE was 7:3) to form a homogeneous slurry, which was spread on a prefabricated gas diffusion layer. The prepared electrode was calcined at 245 °C for 45 min and then at 350 °C for 50 min in nitrogen atmosphere. The cathode was obtained after spraying Nafion solution on the surface of the electrode to form hydrophilic surface with Nafion loading of 0.7 mg cm^{-2}. To form the membrane electrode assembly (MEA), the Nafion 212 was sandwiched between two electrodes and then hot-pressed at 140 °C under 0.2 MPa for 1 min and 1 MPa for 1 min.

2.5.2. Single cell tests

Single cell tests were conducted in a 5 cm^2 single PEMFC which was assembled as reported previously [27]. The single cells were tested at 80 °C with the fuel (H_2) and the oxidant (O_2) humidified by bubbling through distilled water at 90 and 85 °C. The operating gas pressures were kept at 0.2 MPa for both electrodes. The activation of single cell was conducted at 1000 mA cm^{-2} for 8 h. The cells with

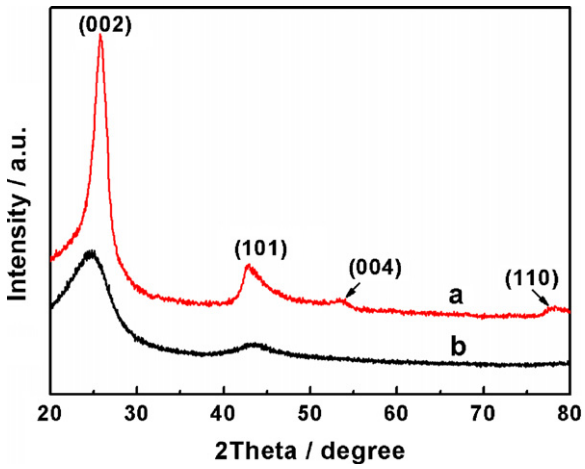

Fig. 1. XRD patterns of (a) GCX and (b) XC-72.

Pt/GCX and Pt/C (20 wt.%) as cathode catalysts were named as cell A and cell B, respectively.

The durability test of cathode catalyst on the single cell performance was carried out by a potential cycling AAT after the measure of the initial performance. The anode and the cathode were injected with hydrogen and nitrogen at 0.2 MPa during the test. In order to simulate the usual PEMFCs operation potential (between the open circuit potential and the normal operation potential), the cathode was subject to a potential scan between 0.6 and 1.2 V versus the anodic potential with the scan rate of 20 mV s^{-1} [27]. The cell performances were recorded before and after 3000 cycles potential sweep test to evaluate the durability of cathode catalyst by comparing the initial and final single cell performances, respectively.

3. Results and discussion

3.1. Surface and structure characteristics

Fig. 1 shows the XRD pattern of the GCX with that of Vulcan XC-72 carbon black (Cabot Corp., denoted as XC-72) as the comparison. The two well-resolved XRD diffraction peaks centered at 2θ of 26.3° and 42.6° which are assigned to (0 0 2) and (1 0 1) diffractions of the graphitic framework are observed for both GCX and XC-72. Moreover, the two peaks of GCX are sharper and narrower than those of XC-72. At the same time two peaks (centered at 53.9° and 77.5°) corresponding to the (0 0 4) and (1 1 0) diffractions for the graphite can also be seen for GCX, which indicates that GCX sample has a high degree of graphitization. The high crystallinity of carbon structure may be directly attributed to the high temperature (1800 °C) in the heat-treatment process [28]. In addition, the presence of cobalt nitrate during the pyrolysis may have some effects on accelerating the graphitize process [23–25].

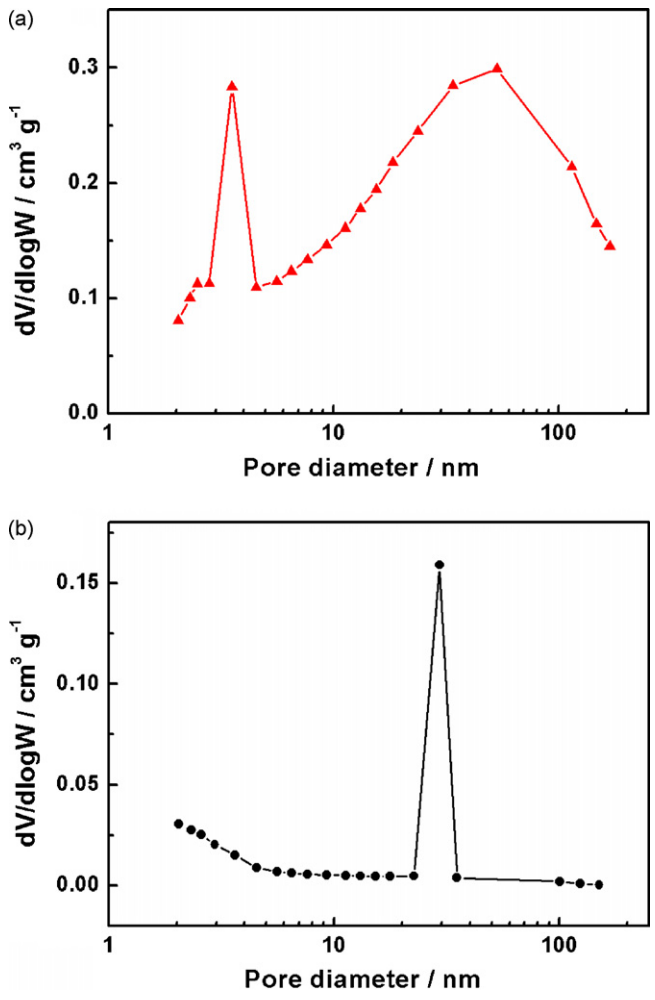

Fig. 2. Pore size distributions of (a) GCX and (b) XC-72.

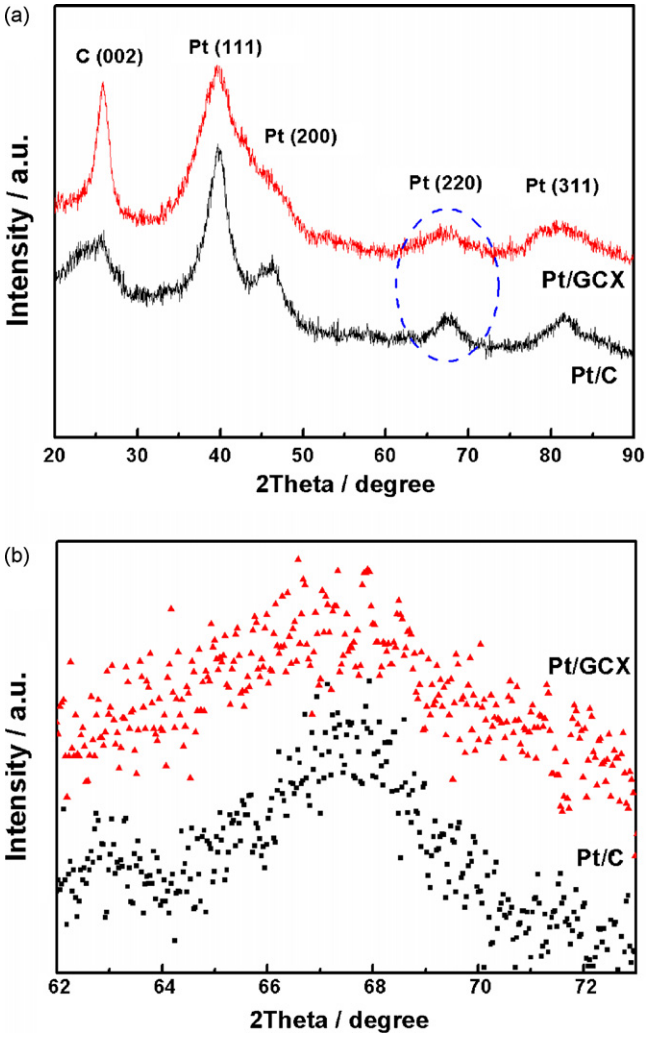

Fig. 3. (a) XRD patterns and (b) enlarged XRD patterns of Pt/GCX and Pt/C.

Table 1
Surface and textural properties of GCX and XC-72.

Sample	BET ($m^2\ g^{-1}$)	V_{total} ($cm^3\ g^{-1}$)	V_{meso} ($cm^3\ g^{-1}$)	V_{micro} ($cm^3\ g^{-1}$)	Pore size (nm)
GCX	143	0.402	0.400	0.008	11.2
XC-72	235	0.554	0.517	0.037	9.4

Fig. 2 displays the pore size distributions (PSDs) of GCX and XC-72. Surface areas and textural characteristics of the GCX and XC-72 are compiled in Table 1. It can be seen in Fig. 2 that the PSD of XC-72 is between 25 and 35 nm, which is in the mesopore range (2–50 nm). Compared with XC-72, the PSDs of GCX sample are in the range of 3–4 and 30–80 nm. It has been reported that the pores with 3–8 nm are useful for fuel diffusion and the pores in the 20–40 nm region are accessible for the Nafion ionomer to contact Pt [28]. Therefore, the special PSDs of GCX are favorable to the ORR and mass-transfer in PEMFCs. As is shown in Table 1, although the BET specific surface area of GCX is 92 $m^2\ g^{-1}$ less than that of XC-72, the mesoporous percentage of GCX calculated to be 99.5% is larger than that of XC-72 (93.3%). The results may be attributed to the elimination of micropore along with the crystallization of carbon structure during the high temperature treatment. Because of its superior mesopore size distribution, GCX is supposed to be a feasible support material for electrocatalysts of PEMFCs.

Fig. 3(a) shows the XRD patterns of Pt/GCX and Pt/C (20 wt.%). The (0 0 2) diffraction of graphitic framework for Pt/GCX centered at 2θ of 26.3° is still obviously sharper and narrower than that of Pt/C, which demonstrates that the original graphitic structure of GCX has not been destroyed in the synthesis of Pt/GCX. The peaks centered at 40.0°, 46.4°, 67.5° and 81.5° are ascribed to Pt (1 1 1), Pt (2 0 0), Pt (2 2 0) and Pt (3 1 1). The Pt (1 1 1) and Pt (2 0 0) peaks of Pt/GCX are almost connected as one peak due to the sharp background peak of GCX support centered at 2θ of 42.6° ((1 0 1) diffraction of graphitic framework). The Pt (2 2 0) peak (2θ of 67.5°) of Pt/GCX is evidently broader than that of Pt/C (20 wt.%). As mentioned above, the face-centered cubic (fcc) reflection patterns of the Pt (2 2 0) diffraction peak suite Gaussian line shapes on a linear background, thus the average particle size of the Pt particles could be estimated from the Pt (2 2 0) diffraction peak in the X-ray diffraction data [26]. From the enlarged image in Fig. 3(b), the average crystallite size of Pt/GCX catalyst was estimated to be smaller than that of Pt/C (20 wt.%).

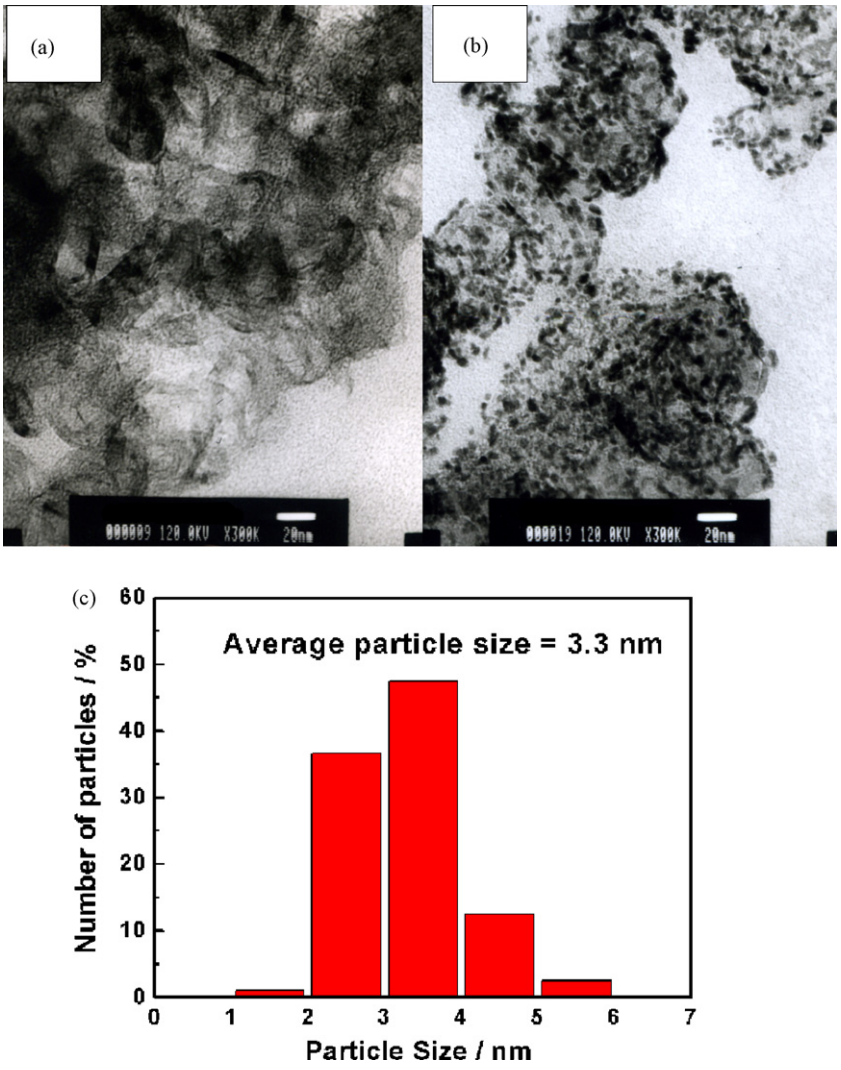

Fig. 4. TEM images of (a) GCX and (b) Pt/GCX. (c) Nanoparticles size histogram of deposited Pt on GCX.

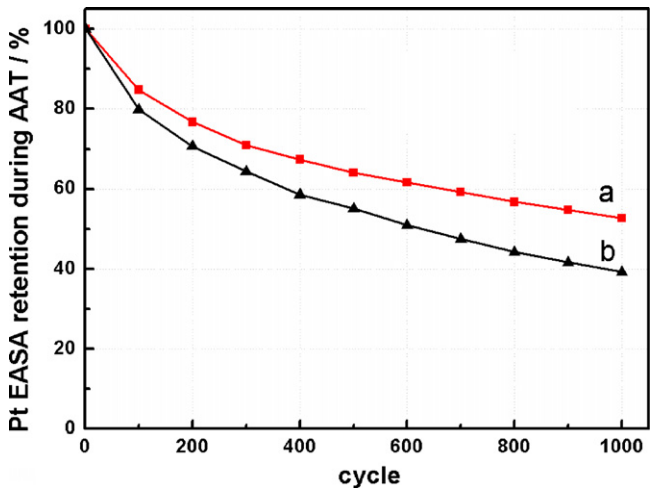

Fig. 5. Electrochemical active surface area retention as a function of cycle number for (a) Pt/GCX and (b) Pt/C catalysts on a glassy carbon electrode.

The TEM images of the GCX and Pt/GCX catalyst are shown in Fig. 4. There is no obvious metal particle in the GCX sample. Coupled with the result of ICP-AES analysis, the cobalt species has been indeed completely removed by being washed with 0.5 M H_2SO_4. The micro-morphology of polyhedral graphitic carbon can be seen in Fig. 4(a). As shown in Fig. 4(b) and (c), the Pt nanoparticles deposited on the GCX are well dispersed and exhibit relatively narrow size distribution with an average particle size of 3.3 nm.

3.2. Electrochemical characteristics

It is revealed that the EASA decreases gradually during the CV continuous cycling as shown in Fig. 5. The Pt EASA retention of Pt/GCX and Pt/C (20 wt.%) was calculated to be 53% and 39% after AAT, indicating that Pt/GCX catalyst potentially presents much better durability than Pt/C (20 wt.%). The ORR polarization curves before and after AAT for Pt/GCX and Pt/C (20 wt.%) are displayed in Fig. 6. The initial half-wave potentials $E_{1/2}$ (the potential corresponding to a half of the diffusion current [27]) of Pt/GCX and Pt/C (20 wt.%) were 809 and 813 mV, while the final (after 1000 cycles potential sweep test) half-wave potentials $E_{1/2}'$ of Pt/GCX and Pt/C (20 wt.%) were 773 and 711 mV. The potential decreases E_d of the two catalysts for ORR activity calculated with the equation $E_d = E_{1/2} - E_{1/2}'$ were 36 and 102 mV, respectively. The results clearly demonstrate that Pt/GCX catalyst maintains a higher activity towards ORR than Pt/C (20 wt.%) after 1000 cycles potential sweep test. One reason for the high stability is that GCX can effectively resist oxidative corrosion due to the high degree of graphitization derived from high temperature treatment. Another reason may be the enhancement of interaction between Pt and GCX support. The π sites of GCX, which are considered the anchoring centers for Pt nanoparticles, are strengthened along with the increase of graphitization [1,19]. Consequently, the agglomeration of GCX supported Pt nanoparticles could be inhibited. So the decrease of EASA and ORR for Pt/GCX is evidently alleviated as well.

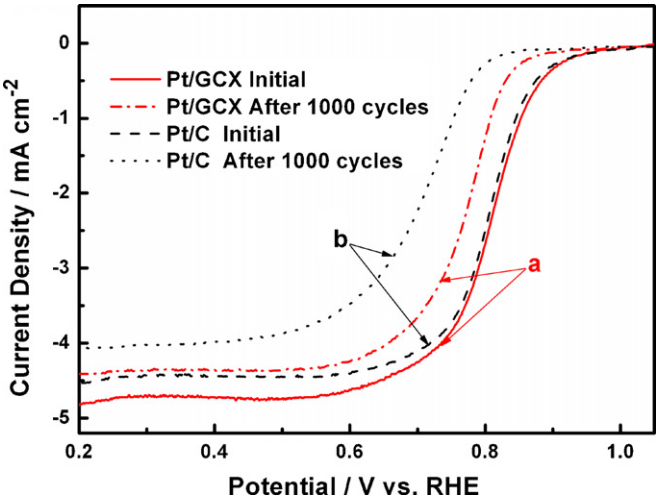

Fig. 6. Polarization curves before and after 1000 cycles of (a) Pt/GCX and (b) Pt/C for ORR in O_2 saturated 0.5 M H_2SO_4 at room temperature. Sweep rate: 1600 rpm.

3.3. Stability tests of single cells

Before and after 3000 cycles potential sweep test, the performances curves of cell A and cell B are recorded and shown in Fig. 7. The initial performance of cell A is higher than that of cell B, which may be attributed to the proper mesopore structure of GCX for mass-transfer and the well dispersion of Pt nanoparticles to provide abundant active sites. The amounts of performance degradation for the two cells at different current densities are compared in Fig. 8. The cell voltage loss of cell A is 12 mV at 100 mA cm^{-2}, which is 50.0% less than that of cell B (24 mV). In addition, the cell voltage loss of cell A is 23 mV at 500 mA cm^{-2}, which is 46.5% less than that of cell B (43 mV).

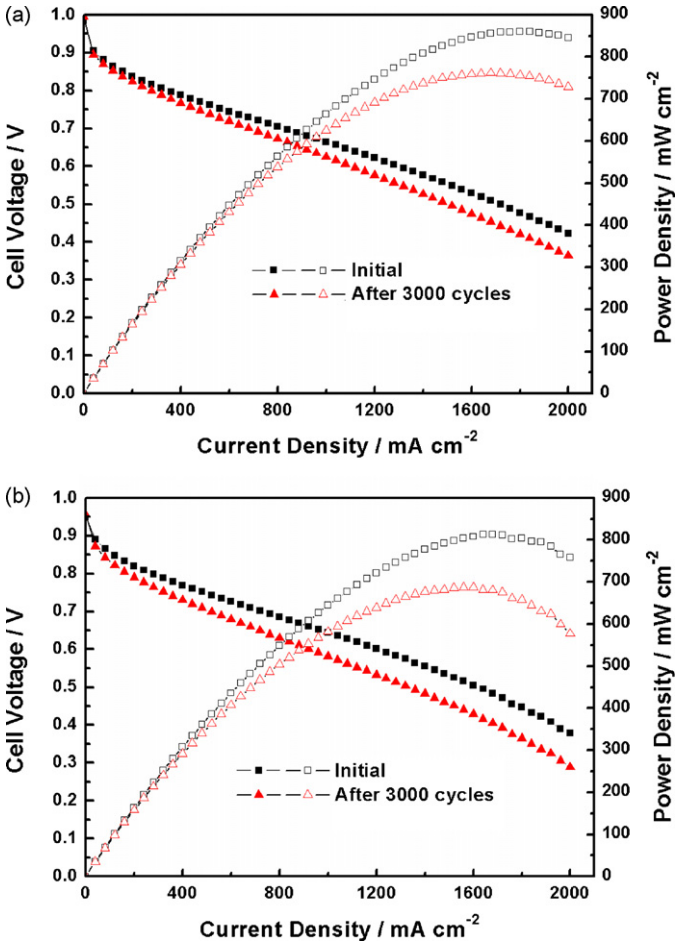

Fig. 7. Single cell performance curves of (a) cell A and (b) cell B before and after the 3000 cycles of potential sweep. *Anode*: The commercial 47.6 wt.% Pt/C with Pt loading of 0.3 mg cm^{-2}. *Cathode*: Pt/GCX or Pt/C (20 wt.%) with Pt loading of 0.3 mg cm^{-2}. $T_{H_2}/T_{cell}/T_{O_2}$ = 90 °C/80 °C/85 °C, P_{H_2}/P_{O_2} = 0.2 MPa/0.2 MPa. *Membrane*: Nafion212 (Du Pont Corp.).

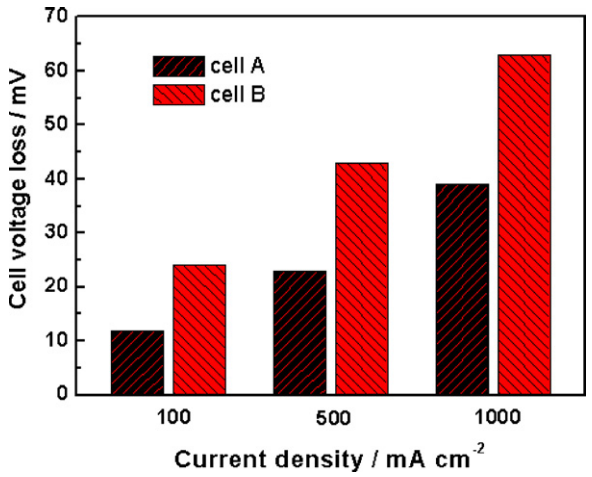

Fig. 8. The cell voltage losses of cell A (Pt/GCX as cathode catalyst) and cell B (Pt/C (20 wt.%) as cathode catalyst) at different current densities.

Compared with the performance degradation of cell B, the smaller voltage loss of cell A indicates that Pt/GCX catalyst possesses better stability than Pt/C (20 wt.%) in single cell tests, which is consistent with the result of electrochemical characterization. The special properties of GCX support play an important role on the long-term operating condition of PEMFCs. As mentioned above, the stable structure and abundant anchoring sites of GCX effectively prevent Pt nanoparticles from agglomerating and detaching from GCX support surface, which contribute to the high corrosion resistance of Pt/GCX.

4. Conclusions

GCX with high degree of graphitization and superior mesopore size distribution was successfully synthesized through a modified sol–gel method followed by high temperature thermal treatment and investigated as support of PEMFCs electrocatalyst. Pt nanoparticles are well dispersed on the GCX and exhibit relatively narrow size distribution with an average nanoparticles size of 3.3 nm. Owing to the better corrosion resistance of GCX and the probable interaction between Pt nanoparticles and GCX support, Pt/GCX catalyst exhibits better stability than Pt/C (20 wt.%) in both electrochemical measurements and single cell tests. Together with its feasible and relatively inexpensive synthesis process, GCX is a promising substitute for the commercial Vulcan XC-72 carbon black as electrocatalyst support in PEMFCs.

Acknowledgement

The authors gratefully acknowledge the financial support by the National High Technology Research and Development Program of China (863 Program, No. 2009AA05Z114).

References

[1] Y. Shao, G. Yin, Y. Gao, J. Power Sources 171 (2007) 558.
[2] S. Knights, K. Colbow, J. St-Pierre, D. Wilkinson, J. Power Sources 127 (2004) 127.
[3] J. Liu, Z. Zhou, X. Zhao, Q. Xin, G. Sun, B. Yi, Phys. Chem. Chem. Phys. 6 (2004) 134.
[4] Y. Shao, G. Yin, J. Zhang, Y. Gao, Electrochim. Acta 51 (2006) 5853.
[5] X. Cheng, L. Chen, C. Peng, Z. Chen, Y. Zhang, Q. Fan, J. Electrochem. Soc. 151 (2004) A48.
[6] K. Kinoshita, J. Bett, Carbon 12 (1974) 525.
[7] X. Yu, S. Ye, J. Power Sources 172 (2007) 145.
[8] T. Ioroi, H. Senoh, S. Yamazaki, Z. Siroma, N. Fujiwara, K. Yasuda, J. Electrochem. Soc. 155 (2008) B321.
[9] X. Cui, L. Guo, F. Cui, Q. He, J. Shi, J. Phys. Chem. C 113 (2009) 4134.
[10] H. Chhina, S. Campbell, O. Kesler, J. Power Sources 161 (2006) 893.
[11] E. Ambrosio, C. Francia, C. Gerbaldi, N. Penazzi, P. Spinelli, M. Manzoli, G. Ghiotti, J. Appl. Electrochem. 38 (2008) 1019.
[12] X. Wang, W. Li, Z. Chen, M. Waje, Y. Yan, J. Power Sources 158 (2006) 154.
[13] X. Wang, M. Waje, Y. Yan, Electrochem. Solid-State Lett. 8 (2005) A42.
[14] T. Yoshitake, Y. Shimakawa, S. Kuroshima, H. Kimura, T. Ichihashi, Y. Kubo, D. Kasuya, K. Takahashi, F. Kokai, M. Yudasaka, S. Iijima, Physica B 323 (2002) 124.
[15] M. Kosaka, S. Kuroshima, K. Kobayashi, S. Sekino, T. Ichihashi, S. Nakamura, T. Yoshitake, Y. Kubo, J. Phys. Chem. C 113 (2009) 8660.
[16] K. Park, Y. Sung, S. Han, Y. Yun, T. Hyeon, J. Phys. Chem. B 108 (2004) 939.
[17] T. Hyeon, S. Han, Y. Sung, K. Park, Y. Kim, Angew. Chem. Int. Ed. 42 (2003) 4352.
[18] G. Chai, S. Yoon, J. Yu, J. Choi, Y. Sung, J. Phys. Chem. B 108 (2004) 7074.
[19] C. Liang, Z. Li, S. Dai, Angew. Chem. Int. Ed. 47 (2008) 3696.
[20] J. Marie, S. Berthon-Fabry, M. Chatenet, E. Chainet, R. Pirard, N. Cornet, P. Achard, J. Appl. Electrochem. 37 (2007) 147.
[21] R. Pekala, J. Mater. Sci. 24 (1989) 3221.
[22] F. Maldonado-Hódar, A. Pérez-Cadenas, C. Moreno-Castilla, Carbon 41 (2003) 1291.
[23] F. Maldonado-Hódar, C. Moreno-Castilla, J. Rivera-Utrilla, Y. Hanzawa, Y. Yamada, Langmuir 16 (2000) 4367.
[24] R. Fu, T. Baumann, S. Cronin, G. Dresselhaus, M. Dresselhaus, J. Satcher, Langmuir 21 (2005) 2647.
[25] F. Maldonado-Hódar, M. Ferro-García, J. Rivera-Utrilla, C. Moreno-Castilla, Carbon 37 (1999) 1199.
[26] V. Radmilović, H. Gasteiger, P. Ross, J. Catal. 154 (1995) 98.
[27] G. Liu, H. Zhang, Y. Zhai, Y. Zhang, D. Xu, Z. Shao, Electrochem. Commun. 9 (2007) 135.
[28] E. Antolini, Appl. Catal. B: Environ. 88 (2009) 1.